frontiers | Frontiers in Materials

TYPE Original Research
PUBLISHED 31 August 2023
DOI 10.3389/fmats.2023.1214426

Check for updates

OPEN ACCESS

EDITED BY
Nafisa Gull,
University of the Punjab, Pakistan

REVIEWED BY
Mojtaba Koosha,
Qilu University of Technology, China
Amir Mohammad Ghadiri,
Sharif University of Technology, Iran
Sumit Sinha Ray,
Indian Institute of Technology Delhi, India

*CORRESPONDENCE
Salema K. Hadrawi,
sahadrawi@gmail.com

RECEIVED 29 April 2023
ACCEPTED 10 August 2023
PUBLISHED 31 August 2023

CITATION
Asiri M, Jawad BahrAluloom Y, Abdullateef Alzubaidi M, Mourad Mohammed I, Suliman M, Ramzy Muhammad E, Abed AS, Abodi Ali F, Hadrawi SK, Alsalamy AH and Alwave M (2023), Synthesis of Cu/Co-hybrid MOF as a multifunctional porous compound in catalytic applications, synthesis of new nanofibers, and antimicrobial and cytotoxicity agents. *Front. Mater.* 10:1214426. doi: 10.3389/fmats.2023.1214426

COPYRIGHT
© 2023 Asiri, Jawad BahrAluloom, Abdullateef Alzubaidi, Mourad Mohammed, Suliman, Ramzy Muhammad, Abed, Abodi Ali, Hadrawi, Alsalamy and Alwave. This is an open-access article distributed under the terms of the Creative Commons Attribution License (CC BY). The use, distribution or reproduction in other forums is permitted, provided the original author(s) and the copyright owner(s) are credited and that the original publication in this journal is cited, in accordance with accepted academic practice. No use, distribution or reproduction is permitted which does not comply with these terms.

Synthesis of Cu/Co-hybrid MOF as a multifunctional porous compound in catalytic applications, synthesis of new nanofibers, and antimicrobial and cytotoxicity agents

Mohammed Asiri[1], Yamamah Jawad BahrAluloom[2], Mazin Abdullateef Alzubaidi[3], Ibrahim Mourad Mohammed[4], Muath Suliman[1], Eman Ramzy Muhammad[5], Ahmed S. Abed[6], Fattma Abodi Ali[7], Salema K. Hadrawi[8]*, Ali H. Alsalamy[9] and Marim Alwave[10]

[1]Department of Clinical Laboratory Sciences, College of Applied Medical Sciences, King Khalid University, Abha, Saudi Arabia, [2]College of MLT, University of Ahl Al Bayt, Kerbala, Iraq, [3]Department of Anesthesia, Al-Mustaqbal University College, Babylon, Iraq, [4]Department of Medicine, Al-Nisour University College, Baghdad, Iraq, [5]Department of Dentistry, AlNoor University College, Bartella, Iraq, [6]Department of Prosthetic Dental Technology, Hilla University College, Babylon, Hillah, Iraq, [7]College of Health Sciences, Medical Microbiology Department, Hawler Medical University, Erbil, Iraq, [8]Refrigeration and Air-conditioning Technical Engineering Department, College of Technical Engineering, The Islamic University, Najaf, Iraq, [9]College of Technical Engineering, Imam Ja'afar Al-Sadiq University, Al-Muthanna, Iraq, [10]Medical Technical College, Al-Farahidi University, Baghdad, Iraq

Several biological properties of metal–organic frameworks (MOFs) and fiber compounds have been reported, and combinations of these structures can have unique properties. In this study, copper-containing and cobalt-containing MOF nanostructures were synthesized by the ultrasonic technique. Then, novel Cu/Co-hybrid MOF nanostructures were synthesized using the ultrasonic method. Synthesized Cu/Co-hybrid MOF nanostructures were used as a new and efficient recyclable catalyst in the synthesis of pyrano[2,3-*c*]pyrazole derivatives using the four-component reaction of phenylhydrazine, ethyl acetoacetate, malononitrile, and aldehyde. In the following, novel Cu/Co-hybrid MOF/PVA (poly vinyl alcohol) fiber nanostructures were synthesized by electrospinning and using Cu/Co-hybrid MOF nanostructures and PVA. The structures of the Cu/Co-hybrid MOF nanostructures and the Cu/Co-hybrid MOF/PVA fiber nanostructures were identified and confirmed using BET, TGA, FTIR, SEM, and XRD. In biological studies, the antibacterial, antifungal, and cytotoxicity activities of Cu/Co-hybrid MOF and Cu/Co-hybrid MOF/PVA fiber nanostructures were evaluated. In investigating the catalytic activity of Cu/Co-hybrid MOF, pyrano[2,3-*c*]pyrazole derivatives were synthesized with higher efficiency and less time than previously reported methods. High antibacterial (against gram-negative and gram-positive strains) and antifungal properties of synthesized Cu/Co-hybrid MOF nanostructures and Cu/Co-hybrid MOF/PVA fiber nanostructures were observed (MIC between 16 and 256 μg/mL), which were higher than some commercial drugs. In the investigation of cytotoxicity activity, the effectiveness on breast cancer cells was studied. The maximum cell

proliferation and viability for Cu/Co-hybrid MOF and Cu/Co-hybrid MOF/PVA fiber nanostructures were 38% and 38% higher than the control in a concentration of 200 µg/mL after 48 h. The high catalytic and biological properties of the synthesized nanoparticles can be attributed to the presence of nano-sized bioactive metals and their high specific surface area. The significant physical-chemical properties obtained for synthesized nanoparticles in this study can be related to the desirable synthesis methods, the development of materials with high purity, and the incorporation of hybrid compounds into the nanostructures.

KEYWORDS

Cu/Co hybrid MOF, catalyst activity, pyrano[2, 3-c]pyrazoles, PVA fiber nanostructures, antibacterial activity, antifungal activity, cytotoxicity activity

1 Introduction

Pyrazole and pyran are two heterocyclic compounds that are abundant in nature. Several biological properties of these compounds have been reported. According to the rules of organic chemistry, the heterocyclic compound created from the connection of these two compounds is known as pyranopyrazole. Several properties that have preserved the biological activities of both these heterocyclic compounds, such as anti-inflammatory and cytotoxicity activities, have been reported in pyranopyrazoles. The most common method of synthesizing these compounds is multicomponent reactions. In multicomponent reactions, where the reactants create the final product in one pot and one step, the catalyst plays an essential role. Therefore, choosing a suitable catalyst is very important in reaction efficiency and product synthesis time (Alam et al., 2015; Garazd and Garazd, 2016; Tipale et al., 2018; Nunes et al., 2020; Sikandar and Zahoor, 2021).

Recently introduced efficient catalysts in the multicomponent synthesis of heterocyclic compounds are metal–organic frameworks (MOFs). MOFs have unique properties due to their high specific surface area and porous structure (Ding et al., 2019). Other applications of MOFs in the fields of medicine, gas storage, and separation (Chen et al., 2020; Wu et al., 2020), preferential gas sorption (Yoon et al., 2010), and photodynamic therapy (Lismont et al., 2017) have been reported. In addition, MOFs containing transition metals such as copper, zinc, and cobalt with cytotoxicity and antimicrobial properties have been reported (Dutta et al., 2019; Ghasemzadeh et al., 2020; Luo et al., 2021; Abdelmoaty et al., 2022; Han et al., 2022).

MOF compounds can be used in the synthesis of nanofibers, which have various applications in medicine and the food industry, such as enzyme stabilization, weaving engineering, wound dressing, and food packaging. Using MOFs to synthesize fiber nanostructures could improve their properties and performance in various fields. The reason can be attributed to the high specific surface area and the bioactivity of some metals that are present in the structure of MOFs (Beter et al., 2017; Kalwar and Shen, 2019; Maliszewska and Czapka, 2022). A literature review showed that copper-containing MOFs and cobalt-containing MOFs have different biological and catalytic properties (Hatamie et al., 2019; Zha et al., 2020; Abdelmoaty et al., 2022; Dong et al., 2022).

Fiber compounds can be synthesized using different materials. Electrospinning is fast developing in several directions (Sridhar et al., 2011). One is fiber creation on an industrial scale, which has been mentioned in many articles. Another is a preparation of complicated structures such as core–shell, Janus, tri-layer core–shell, and 3-section Janus and their combinations from the multiple-fluid processes. The third is the combination of electrospinning with other traditional and advanced chemical methods, such as cross-linking and chemical synthesis, and physical methods, such as 3-D printing (Teixeira et al., 2012; Zhang et al., 2017; Gholami et al., 2020; Kang et al., 2020; Wang et al., 2020; Adamu et al., 2021; Jasim et al., 2022; Liu et al., 2022; Zhao et al., 2022; Zhou et al., 2022; Ge et al., 2023; Liu et al., 2023; Wang et al., 2023; Yu et al., 2023). By using MOF compounds and polyvinyl alcohol with electrospinning methods, various compounds with different applications can be synthesized. For example, poly vinyl alcohol (PVA)/Ag-MOF has been reported with antibacterial activity (Zhang et al., 2021). Another example is Zn-MOF/PVA nanofibers, which has been reported for arsenic removal (Shahryari et al., 2020).

There have been reports of the synthesis of copper-containing MOFs and cobalt-containing MOFs with biological properties and other applications. In addition, with electrospinning technology, it is possible to prepare fibers containing these two nanostructures so that the final synthetic product has the potential biological properties of both MOF compounds. In this study, new Cu/Co-hybrid MOF nanostructures and Cu/Co-hybrid MOF/PVA fiber nanostructures were synthesized. The catalytic activity of Cu/Co-hybrid MOF nanostructures in the synthesis of pyrano[2,3-*c*]pyrazole derivatives was evaluated. Biological evaluations of Cu/Co-hybrid MOF nanostructures and Cu/Co-hybrid MOF/PVA fiber nanostructures, such as cytotoxicity effects, antibacterial effects, and antifungal effects, were performed. Although there have been reports of the synthesis of MOF compounds and fibers with different properties (Azizabadi et al., 2021a; Gecgel et al., 2022; Maliszewska and Czapka, 2022), the advantages and novelty of this study are the synthesis and reporting of a new nanostructure with several diverse catalytic and biological properties. The type of polymer (PVA) was selected based on the biocompatibility properties, the ability to form fibers, and the inherent nature of the polymer.

2 Materials and methods

2.1 Materials, solvents, and device

All raw materials and solvents for the synthesis of the desired compounds, for example, dipicolinic acid

(Mw 0.167 mg $mmol^{-1}$), copper II) nitrate trihydrate (Mw 0.242 mg $mmol^{-1}$), cobalt (II) nitrate hexahydrate (Mw 291.03 g mol^{-1}), and polyvinyl alcohol (Mw 9,000–10,000, 80% hydrolyzed) with high purity, were obtained from Sigma and Merck.

Micromeritics ASAP 2460 was used for N_2 adsorption/desorption. A PerkinElmer TGA 8000 system was used to measure thermal behavior. FT-IR spectra were prepared using a Bruker Tensor 27 FT-IR instrument. XRD patterns were prepared using a Bruker D8 X-ray diffractometer. SEM images of synthesized nanostructures were prepared using a Hitachi S-4800 FESEM instrument. ^{1}H NMR (300 MHz) and ^{13}C NMR (75 MHz) spectra in DMSO-d6 were obtained using a Bruker Ultra Shield-300 instrument. A Kruss KSP1N melting point meter was used to determine the melting point of derivatives. Elemental analysis of derivatives was measured using a PerkinElmer 2400 series II instrument. A Unico S2150 spectrophotometer was used to prepare the concentration of bacterial and fungal suspensions.

2.2 Synthesis of copper-containing MOF nanostructures

In a Pyrex tube, 30 mL double-distilled water, 0.835 g dipicolinic acid (5 mmol), and 1.208 g cupric nitrate (5 mmol) were added. The mixture was irradiated with 20 kHz ultrasonic waves at a power of 220 W and temperature of 60°C for 20 min. The obtained sediments were separated by centrifugation and washed three times with water and ethanol. Finally, the obtained copper-containing MOF nanostructures were dried under vacuum for 48 h at room temperature (Ahmad et al., 2022).

2.3 Synthesis of cobalt-containing MOF nanostructures

In a Pyrex tube, 30 mL double-distilled water, 0.835 g dipicolinic acid (5 mmol), and 0.915 g cobalt nitrate (5 mmol) were added. Other steps to the synthesis and purification of cobalt-containing MOF nanostructures were similar to copper-containing MOF nanostructures (Ahmad et al., 2022).

2.4 Synthesis of Cu/Co-hybrid MOF nanostructures

In separate containers, 0.05 g of copper-containing MOF nanostructures was dissolved in acetic acid (30 mL), and 0.05 g of cobalt-containing MOF nanostructures was dissolved in acetic acid (30 ml). The contents of the two containers were mixed and stirred at a temperature of 70°C until a homogeneous mixture was reached. Then, the mixture was irradiated with 20-kHz ultrasonic waves at a power of 220 W and room temperature for 20 min. Finally, the obtained sediments were separated by centrifugation and dried under a vacuum (Cui et al., 2023; Yang et al., 2023).

2.5 Catalyst activity of Cu/Co-hybrid MOF nanostructures

2.5.1 General method for synthesis of pyrano[2,3-c] pyrazole using Cu/Co-hybrid MOF nanostructures

In the mixture of 2 mL EtOH: H_2O (1:1), 1 mmol phenylhydrazine, 1 mmol ethyl acetoacetate, and 3 mg of Cu/Co-hybrid MOF nanostructures were stirred at 40°C. The reaction was monitored by thin layer chromatography (TLC), and after completion, 1 mmol malononitrile and 1 mmol aromatic aldehydes were added and stirred under the same conditions mentioned previously. After completion of the reaction, which was monitored by TLC, cold contents to the room temperature and and 10 mL of acetone were added. Cu/Co-hybrid MOF nanostructures were collected by nanofiltration, and after removing the solvent in a vacuum, the synthesized pyrano[2,3-*c*]pyrazole derivatives were recrystallized in a mixture of EtOH: H_2O (1:1).

2.5.2 Synthesis of pyrano[2,3-c]pyrazole derivatives using Cu/Co-hybrid MOF nanostructures

To use Cu/Co-hybrid MOF nanostructures as a catalyst for the synthesis of pyrano[2,3-*c*]pyrazole derivatives, first, the solvent and amount of catalyst were optimized (Table 2). Other derivatives were synthesized using optimal conditions (Table 3). After the pyrano [2,3-*c*]pyrazole derivatives were synthesized, the separated catalyst was washed three times with water and ethanol and dried at room temperature for 48 h. After drying, it was reused. The catalyst recycling results for 5a are given in Figure 10. The catalytic properties of Cu/Co-hybrid MOF nanostructures for the synthesis of pyrano[2,3-*c*]pyrazole derivatives are compared to previous reports in Table 4.

6-amino-4-(4-hydroxy-3-methoxyphenyl)-3-methyl-1-phenyl-1,4-dihydropyrano[2,3-c]pyrazole-5-carbonitrile (5g).

^{1}H NMR (300 MHz, DMSO-d6) δ = 1.75 (s, 3H, CH_3), 3.67 (s, 3H, OCH_3), 4.82 (s, 1H, CH), 6.63 (d, 1H, J = 8.4 Hz, Ar-H), 6.60 (s, 1H, Ar-H), 6.73 (d, 1H, J = 8.4 Hz, Ar-H) 7.26 (s, 2H, NH_2), 7.41–7.72 (m, 5H, Ar-H), and 8.67 (s, 1H, OH);

^{13}C NMR (75 MHz, DMSO-d6) δ = 13.6, 36.4, 55.6, 99.3, 112.5, 115.1, 117.4, 120.5, 121.2, 126.4, 129.1, 130.5, 135.6, 138.2, 144.4, 146.5, 147.8, 152.6, and 160.9;

TABLE 1 BET, BJH pore volume, and mean pore diameter of copper-containing MOF nanostructures (I), cobalt-containing MOF nanostructures (II), Cu/Co-Hybrid MOF nanostructures (III), and Cu/Co-hybrid MOF/PVA fiber nanostructures (IV).

Sample	BET (m^3/g)	BJH volume pore (cm^3/g)	Mean pore diameter (nm)
Copper-containing MOF nanostructures	1103	0.35	1.22
Cobalt-containing MOF nanostructures	1024	0.21	1.56
Cu/Co-hybrid MOF nanostructures	1247	0.42	1.73
Cu/Co-hybrid MOF/ PVA fiber nanostructures	1570	0.49	1.92

TABLE 2 Optimization of reaction conditions in synthesis of pyrano[2,3-*c*]pyrazoles using Cu/Co-hybrid MOF nanostructures as a catalyst (5a).

No.	Solvent	Catalyst (mg)	Temperature (°C)	Time (min)	Yield (%)
1	H_2O	1	40	30	56
2	EtOH	1	40	30	51
3	H_2O:EtOH (1:1)	1	40	20	73
4	MeOH	1	40	30	34
5	H_2O:EtOH (1:1)	2	40	15	86
6	H_2O:EtOH (1:1)	3	40	10	94
7	H_2O:EtOH (1:1)	4	40	10	94
8	H_2O:EtOH (1:1)	5	40	15	89
9	H_2O:EtOH (1:1)	3	r. t	60	66
10	H_2O:EtOH (1:1)	3	50	10	92
11	H_2O:EtOH (1:1)	3	60	15	90
12	H_2O:EtOH (1:1)	3	70	20	86
13	H_2O:EtOH (1:1)	3	reflux	30	77

Reaction conditions for synthesis of 5a: 1 mmol phenylhydrazine, 1 mmol ethyl acetoacetate, 1 mmol malononitrile, and 1 mmol benzaldehyde.

TABLE 3 Synthesized 1,4-dihydropyrano[2,3-c]pyrazole derivatives (5a-n).

Entry	Product	Aldehyde derivative	Reaction time (min)	Isolated yield (%)	Melting point (°C)	
					Found	Reported Eftekhari far and Nasr-Esfahani, (2020)
1	**5a**	C_6H_5	10	94	165–167	167–169
2	**5b**	3-NO_4-C_6H_4	15	92	188–189	189–191
3	**5c**	4-NO_4-C_6H_4	10	95	190–192	191–193
4	**5d**	4-CH_3-C_6H_4	25	90	172–173	173–175
5	**5e**	4-OCH_3-C_6H_4	10	94	168–169	169–171
6	**5f**	4-OH-C_6H_4	30	89	207–210	208–210
7	**5g**	4-OMe,4-OH-C_6H_3	30	87	181–183	182–184
8	**5h**	4-CN-C_6H_4	25	91	195–196	194–196
9	**5i**	2-Cl-C_6H_4	20	91	141–143	143–145
10	**5j**	2,4-Cl-C_6H_3	20	92	182–184	181–183

Reaction conditions: 1 mmol phenylhydrazine, 1 mmol ethyl acetoacetate, 1 mmol malononitrile, 1 mmol aromatic aldehydes, and 2 mg Cu/Co-hybrid MOF nanostructures in 2 mL EtOH: H_2O (1:1) at 40 C.

Anal. Calcd for $C_{21}H_{18}N_4O_3$: C, 67.37; H, 4.85; N, 14.96; and O, 12.82. Found: C, 67.39; H, 4.97; N, 14.93; and O, 12.81.

2.6 Synthesis of Cu/Co-hybrid MOF/PVA fiber nanostructures

Cu/Co-hybrid MOF/PVA fiber nanostructures were prepared by the electrospinning method under optimal conditions. According to reported methods (Sargazi et al., 2019; Azizabadi et al., 2021b), in 25 mL distilled water, 0.01 mg of Cu/Co-hybrid MOF nanostructures were dissolved (Sol. A). In another solution (Sol. B), 0.004 g PVA (polyvinyl alcohol) was dissolved in 20 mL acetic acid. Sol. A was added to Sol. B under magnetic stirring for 20 min at 80°C. Finally, the electrospinning parameters of 28 kV, 22 cm spinning distance, and 0.4 mL/h flow rate were used to successfully synthesize Cu/Co-hybrid MOF/PVA fiber nanostructures (Sargazi et al., 2019; Azizabadi et al., 2021b) Figure 1.

2.7 Characterization of synthesized nanostructures

The synthesized nanostructures were characterized using BET (N_2 adsorption/desorption isotherms) technique, TGA (thermal behavior), FTIR (infrared spectroscopy), SEM (scanning electron

TABLE 4 Comparison of synthesis of pyrano[2,3-*c*]pyrazoles (5a) in different conditions.

Entry	Catalyst	Temperature (°C)	Solvent/condition	Time (min)	Yield (%)
1	Nano-FDP	100	H_2O/Ultrasonication	4	95 Dam et al. (2015)
2	Uncapped SnO_2 NPs	r. t	H_2O	150	93 Paul et al. (2014)
3	Sulfonic acid immobilization on NPs	Reflux	H_2O:EtOH(1:1)	40	93 Eftekhari far and Nasr-Esfahani, (2020)
4	Yttrium iron garnet NPs	80	Solvent-free	20	91 Sedighinia et al. (2019)
5	Cetyltrimethylammonium bromide	90	H_2O	240	89 Wu et al. (2013)
6	Triphenylphosphine	Reflux	(H_2O)	120	87 Amine Khodja et al. (2016)
7	Cu/Co-hybrid MOF nanostructures	40	H_2O:EtOH(1:1)	10	94

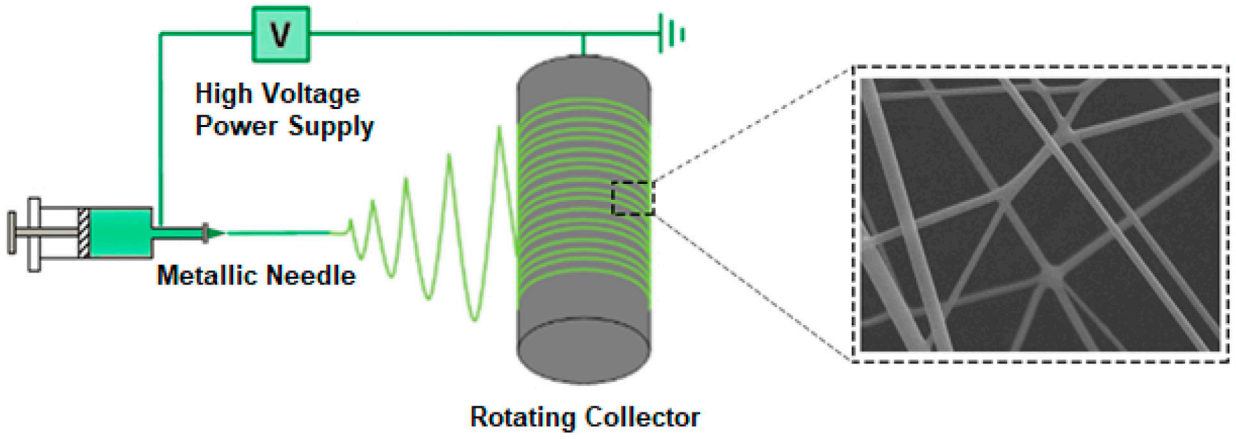

FIGURE 1
Schematic representation of the synthesis of Cu/Co-hybrid MOF/PVA fiber nanostructures.

microscopy), XRD (X-ray diffraction) patterns, contact angle, compressive strength, and flexural strength.

2.8 Cytotoxicity activity

MCF-7 breast cancer cells (ATCC HTB-22) were cultured for 2 weeks in a control medium containing RPMI 1640, FBS (10%), and streptomycin (100 μg mL^{-1})/penicillin G (100 μg mL^{-1}). Then, MCF-7 breast cancer cells with a cell density of 1.2×10^4 cells were seeded in 96-well plates and incubated for 24 h at 37°C and 5% CO_2. After that, 5–200 μg/mL (5, 10, 20, 40, 80, 120, and 200) concentrations of Cu/Co-hybrid MOF nanostructures and Cu/Co-hybrid MOF/PVA fiber nanostructures were added to the wells. They were treated for 24 h and 48 h in the aforementioned conditions. After that time, the media containing Cu/Co-hybrid MOF nanostructures and Cu/Co-hybrid MOF/PVA nanostructures were removed, and 50 μL of MTT solutions (2 mg/mL in PBS) and 150 μL fresh media were added to wells. They were incubated for 4 h in the conditions mentioned previously. Then, the contents of the wells were removed. Finally, 200 μL DMSO was added to the wells, and the absorbance was read at 570 nm (Almajhdi et al., 2014; Heidari Majd et al., 2017; Mu and Wu, 2017; Bonan et al., 2019; Moghaddam-manesh et al., 2021; Moghaddam-Manesh and Hosseinzadegan, 2021).

2.9 Antibacterial and antifungal activities

CLSI (Clinical & Laboratory Standards Institute), guidelines M07-A9 and M27-A2 for MIC (minimum inhibitory concentration) tests and CLSI guideline M26-A for MBC (minimum bactericidal concentration) tests and MFC (minimum fungicidal concentration) tests were used to determine antimicrobial activity (antibacterial against *Bacillus cereus*, *Staphylococcus aureus*, *Streptococcus pyogenes*, *Proteus mirabilis*, *Escherichia coli*, and *Acinetobacter baumannii*; and antifungal activity against *Fusarium oxysporum*, *Candida albicans*, and *Aspergillus fumigatus*) (Hosseinzadegan et al., 2020; Zeraati et al., 2022). For antibacterial activity, the effects of copper-containing MOF nanostructures, cobalt-containing MOF nanostructures, and Cu/Co-hybrid MOF/PVA fiber nanostructures on gram-positive and gram-negative species were evaluated (Hosseinzadegan et al., 2020; Zeraati et al., 2022).

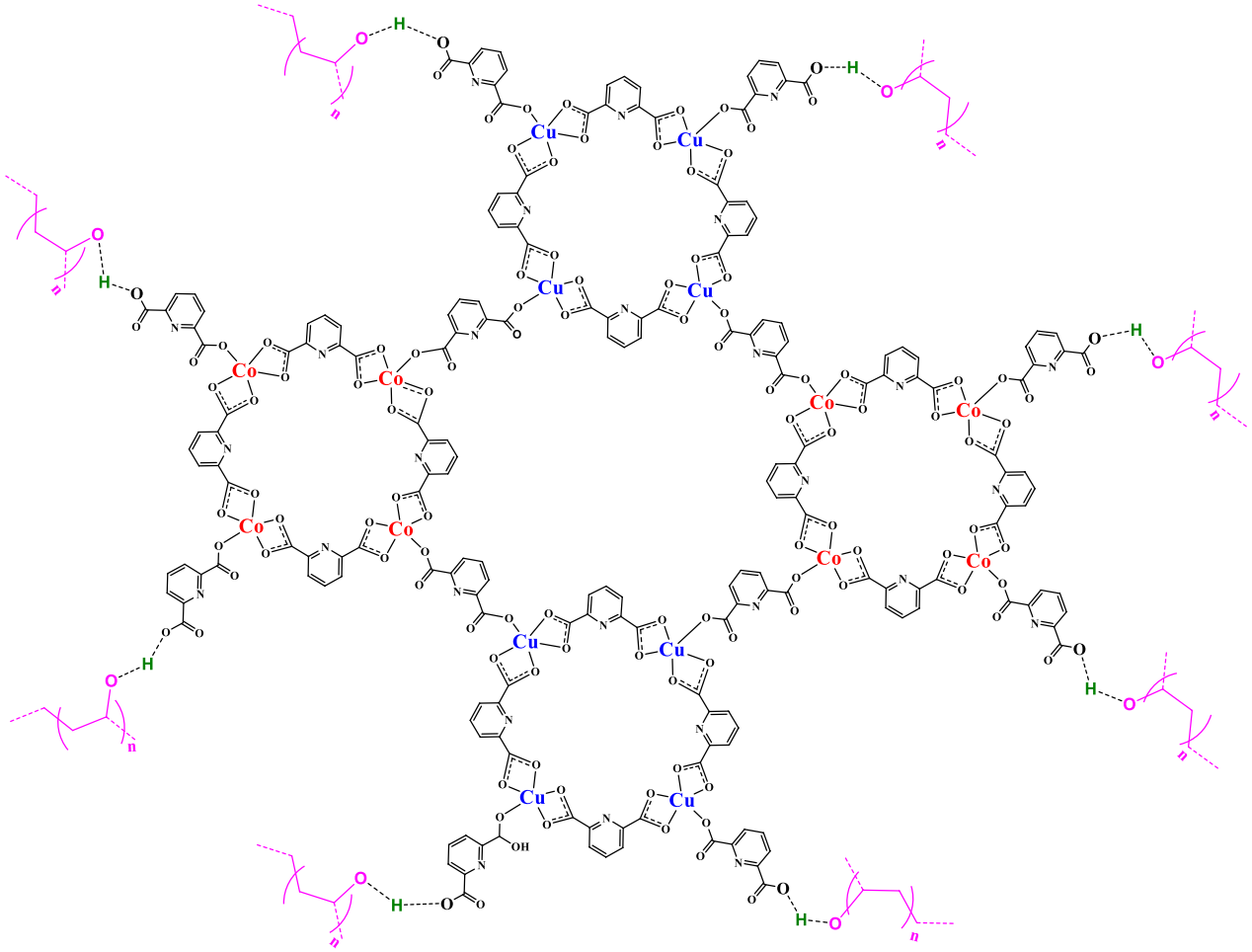

FIGURE 2
Proposed structure for Cu/Co-hybrid MOF/PVA fiber nanostructures.

3 Results

3.1 Identification and characterization of Cu/Co-hybrid and Cu/Co-hybrid MOF/PVA fiber nanostructures

The proposed structure for Cu/Co-hybrid and Cu/Co-hybrid MOF/PVA fiber nanostructures is given in Figure 2. The structure of the Cu/Co-hybrid MOF/PVA fiber network by was identified and characterized by BET (N_2 adsorption/desorption isotherms) technique, TGA (thermal behavior), FTIR (infrared spectroscopy), SEM (scanning electron microscopy), and XRD (X-ray diffraction) patterns.

Figure 3 shows the N_2 adsorption/desorption of copper-containing MOF nanostructures A), cobalt-containing MOF nanostructures B), Cu/Co-hybrid MOF nanostructures C), and Cu/Co-hybrid MOF/PVA fiber nanostructures D). As can be seen, classical isotherms of all compounds were similar to the fourth type (Asiri et al., 2022). The obtained values of specific surface area for copper-containing MOF nanostructures, cobalt-containing MOF nanostructures, Cu/Co-hybrid MOF nanostructures, and Cu/Co-hybrid MOF/PVA fiber nanostructures based on the BET technique were 1103 m^2/g, 1024 m^2/g, 1247 m^2/g, and 1570 m^2/g, respectively.

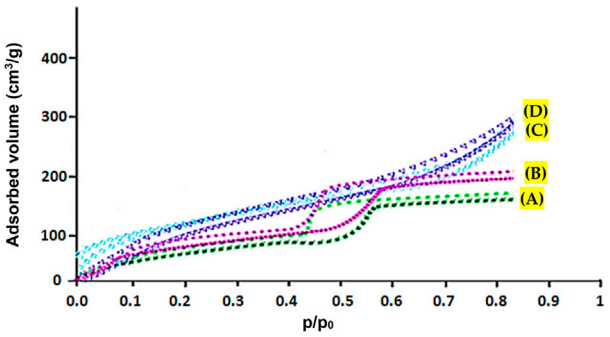

FIGURE 3
N_2 adsorption/desorption of copper-containing MOF nanostructures **(A)**, cobalt-containing MOF nanostructures **(B)**, Cu/Co-hybrid MOF nanostructures **(C)**, and Cu/Co-hybrid MOF/PVA fiber nanostructures **(D)**.

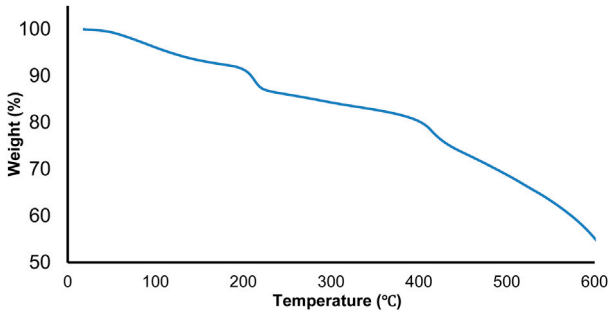

FIGURE 4
Thermal behavior of Cu/Co-hybrid MOF/PVA fiber nanostructures.

According to Table 1, Cu/Co-hybrid MOF/PVA fiber nanostructures have higher surface area and high porosity than copper-containing MOF nanostructures, cobalt-containing MOF nanostructures, and Cu/Co-hybrid MOF nanostructures. This finding could be related to the significant effects of hybrid features on the textural behavior of final products. This capability can affect the application of this material in different fields, such as novel candidates as antimicrobial and antifungal agents.

Synthesis of fiber nanostructures from hybrid MOF nanostructures can increase the specific surface area.

The high specific surface area gives unique capabilities to compounds. Because the high specific surface area causes more contact with the active parts of the compound, the performance of the compound in terms of its biological activity increases(Asgari et al., 2022; Sheta et al., 2022).

The TGA curve of Cu/Co-hybrid MOF/PVA fiber nanostructures is given in Figure 4. The thermal behavior of synthesized fibers nanostructures to 600°C was investigated. The complete decomposition of the compound occurred at a temperature of 418°C. The weight loss at 213°C and 115°C can be related to the loss of fiber connection with the hybrid and the evaporation of nanostructured surface water, respectively.

The synthesized Cu/Co-hybrid MOF/PVA fiber nanostructures have excellent thermal stability to perform biological activities.

In the FT-IR spectrum of synthesized Cu/Co-hybrid MOF/PVA fiber nanostructures (Figure 5), O-H absorption was observed at 3456 cm^{-1} (in PVA). Absorptions observed at 2918 cm^{-1}, 1654 cm^{-1}, 1592 cm^{-1}, 1334 cm^{-1}, and 1161 cm^{-1} can be attributed to C-H (in PVA), C=O (in MOF), C=N (in MOF), C-C (in MOF), and C-O (in MOF), respectively. Absorptions below 1000 cm^{-1} were related to the metal–oxygen. For example, absorptions observed at 600–800 cm^{-1} were due to Co-O (in MOF) (Salavati-Niasari et al., 2009), and absorptions observed in areas 400–600 cm^{-1} were due to Cu-O (in MOF) (Elango et al., 2018).

All peaks of the raw materials were observed in the FT-IR spectrum of Cu/Co-hybrid MOF/PVA fiber nanostructures.

The SEM images of copper-containing MOF nanostructures A), cobalt-containing MOF nanostructures B) (Patra et al., 2022), Cu/Co-hybrid nanostructures C), and Cu/Co-hybrid MOF/PVA fiber nanostructures D) are given in Figure 6. According to the results, the size distribution of copper-containing MOF and cobalt-containing MOF nanostructures is almost the same (between 45 and 55 nm). Meanwhile, based on image C), the particle size distribution for Cu/Co-hybrid nanostructures is around 20 nm. This distribution is less than compound I and II. The difference between the size distributions of compounds A, B, and C can be related to the efficient effects of hybrid nanostructures on the final products. According to the SEM image of compound IV, the mean

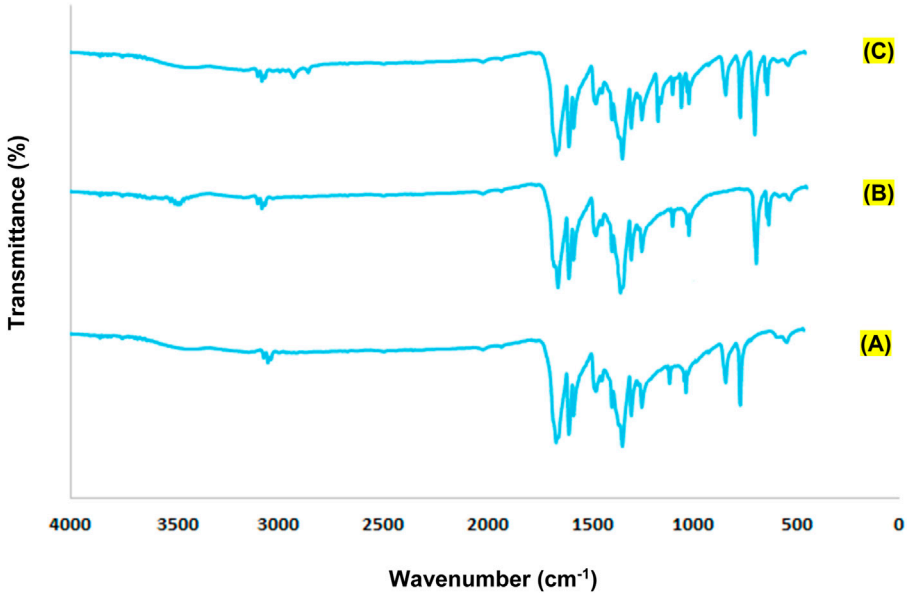

FIGURE 5
FTIR spectra of cobalt-containing MOF nanostructures **(A)**, copper-containing MOF nanostructures **(B)**, and Cu/Co-hybrid MOF/PVA fiber nanostructures **(C)**.

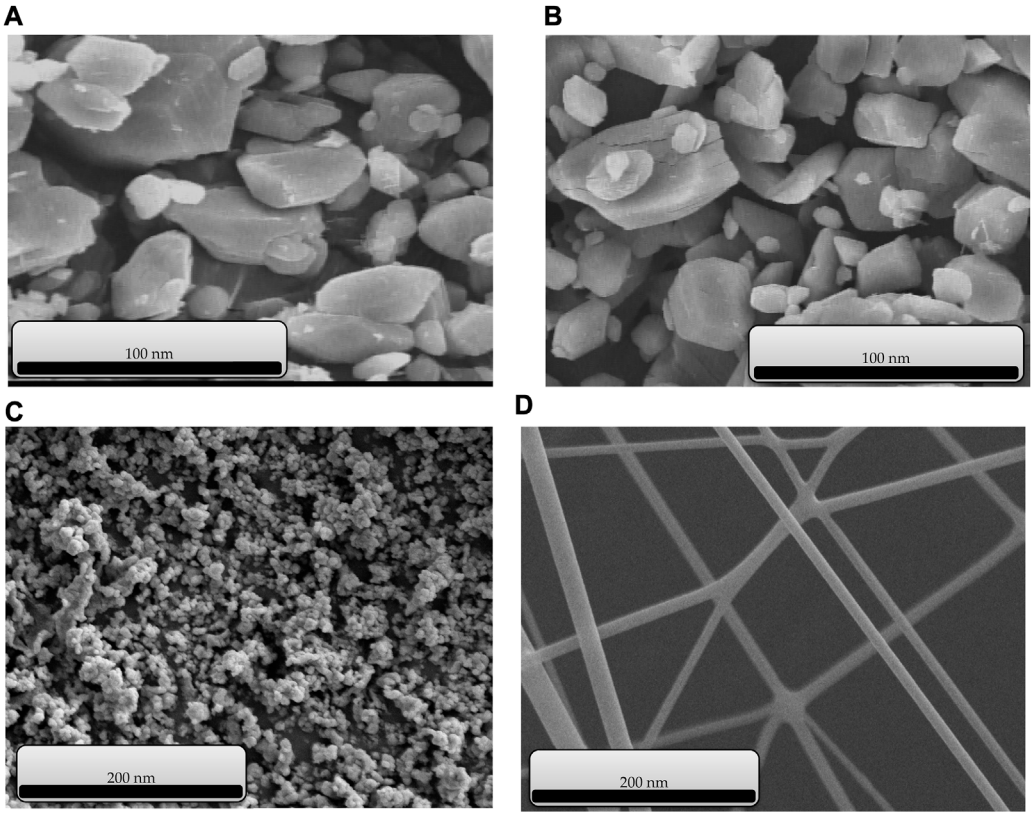

FIGURE 6
SEM images of copper-containing MOF nanostructures **(A)**, cobalt-containing MOF nanostructures **(B)**, Cu/Co-hybrid nanostructures **(C)**, and Cu/Co-hybrid MOF/PVA fiber nanostructures **(D)**.

diameter of fibers in Cu/Co-hybrid MOF/PVA fiber nanostructures is approximately 10 nm. The successful synthesis of Cu/Co-hybrid MOF/PVA fiber nanostructures with narrow fibrous distribution can be related to the effects of optimized electrospinning conditions and combining hybrid features in the final products. The temperature of the electrospinning solution (see Section 2.6) increases the evaporation rate and also changes the viscosity of the polymer solution. Increasing the temperature allows the Coulomb forces to exert more tension on the polymer molecules. As a result, more uniform fibers with smaller diameters are obtained.

The optimal method of synthesizing the compound is suitable, and it leads to the same morphology in the nanorange when synthesizing similar compounds.

Another technique used to identify and confirm the structure of synthesized Cu/Co-hybrid MOF nanostructures and Cu/Co-hybrid MOF/PVA fiber nanostructures was the XRD pattern (Figure 7). The XRD patterns of Cu/Co-hybrid MOF nanostructures A) and Cu/Co-hybrid MOF/PVA fiber nanostructures B) are given in Figure 6. According to the XRD pattern of the final product, peaks related to copper-containing MOF nanostructures (Akhavan-Sigari et al., 2022) and cobalt-containing MOF nanostructures (Shahryari et al., 2022) were observed in these patterns. According to the Debye–Scherrer equation, the average crystalline size in the Cu/Co-hybrid MOF nanostructures is 62 nm, while this size is 45 nm in the Cu/Co-hybrid MOF/PVA fiber nanostructures. This difference in the size of the crystals can relate to the fibrous network of final products (Sadasivan et al., 2013; Uddin and Baig, 2019). This stable network affects the physicochemical properties of nanostructures and produces optimal samples in environmental conditions (Elango et al., 2018).

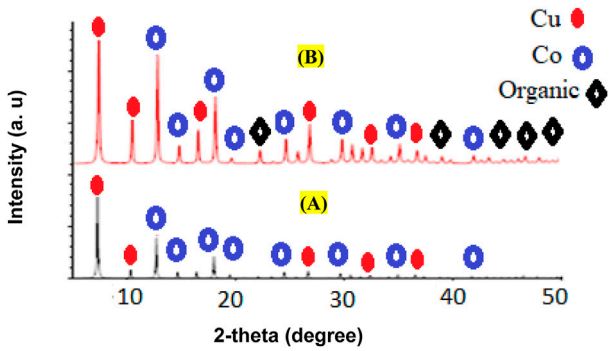

FIGURE 7
XRD patterns of Cu/Co-hybrid MOF nanostructures **(A)** and Cu/Co-hybrid MOF/PVA fiber nanostructures **(B)**.

10.3389/fmats.2023.1214426

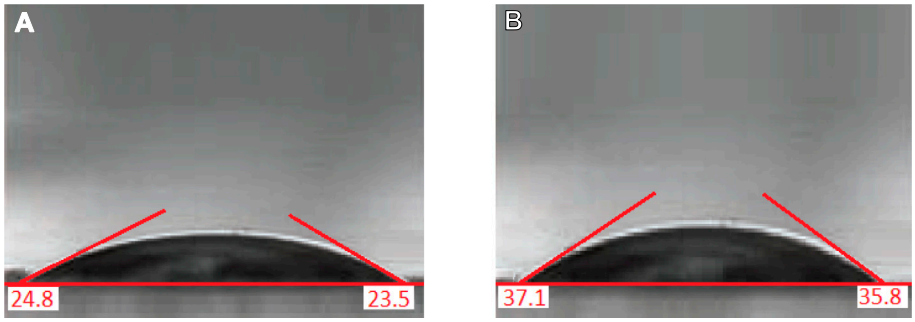

FIGURE 8
Contact angle of Cu/Co-hybrid MOF/PVA fiber nanostructures **(A)** and PVA fiber nanostructures **(B)**.

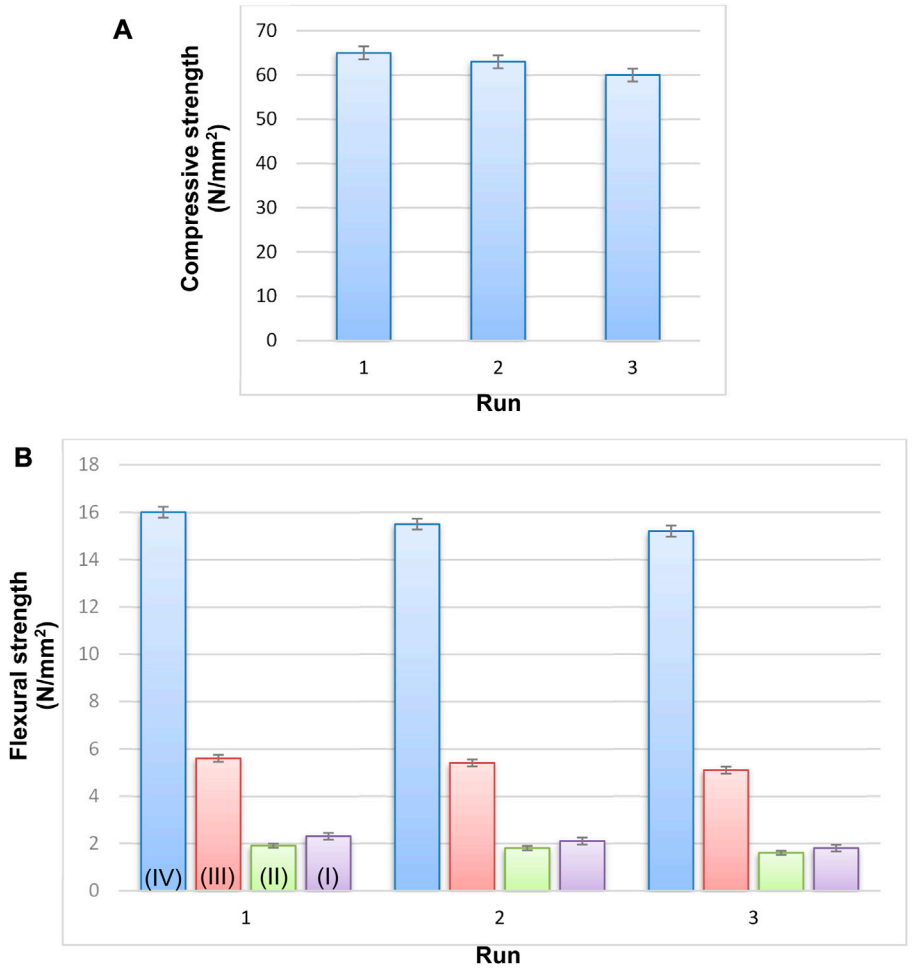

FIGURE 9
Strength of Cu/Co-hybrid MOF/PVA fiber nanostructures **(A)** and flexural strength **(B)** of copper-containing MOF nanostructures (I), cobalt-containing MOF nanostructures (II), Cu/Co-hybrid nanostructures (III), and Cu/Co-hybrid MOF/PVA fiber nanostructures (IV) (n = 3) ± SD.

Using XRD patterns based on the Debye–Hückel equation, the sizes of Cu/Co-hybrid MOF nanostructures and Cu/Co-hybrid MOF/PVA fiber nanostructures were calculated as 44 nm and 56 nm, respectively.

The contact angle method was used to determine the hydrophilicity of Cu/Co-hybrid MOF/PVA nanofibers. In previous studies, the contact angle for polyvinyl alcohol nanofibers has been reported as 35° (Ngadiman et al., 2015). The contact angle for Cu/Co-hybrid MOF/PVA was about 24°. To compare the amount of hydrophilicity, the contact angle for polyvinyl alcohol nanofibers studied was about 36° (Figure 8).

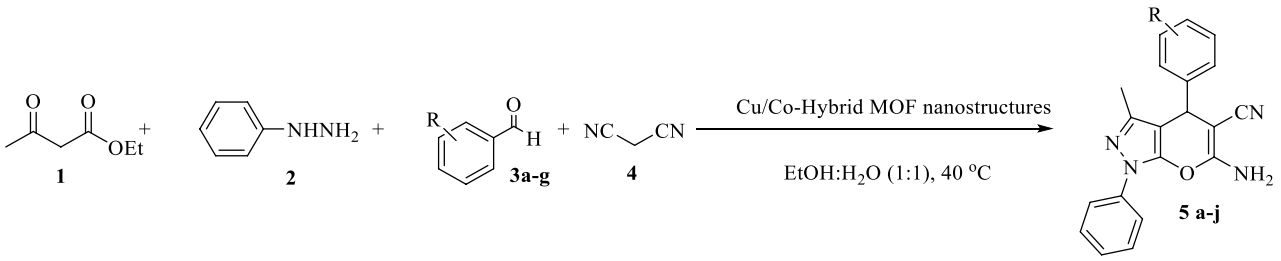

SCHEME 1
Synthesis of pyrano[2,3-*c*]pyrazole derivatives using Cu/Co-hybrid MOF nanostructures as a catalyst.

As we know, a decrease in the contact angle indicates an increase in the hydrophilicity of the compounds. The increased hydrophilicity of synthesized Cu/Co-hybrid MOF/PVA fiber nanostructures compared to polyvinyl alcohol nanofibers can be attributed to the presence of Cu/Co-hybrid MOF in the composition structure, which can establish hydrogen bonds with water molecules (Drelich et al., 2019; Hassan et al., 2019).

Compressive strength and flexural strength tests were used to better characterize the Cu/Co-hybrid MOF/PVA fiber nanostructures.

The result of the compressive strength tests for Cu/Co-hybrid MOF/PVA fiber nanostructures is shown in Figure 9A. According to data, the product has a compressive strength of 65 N/mm^2. This amount can be related to the nature of fibrous polymeric compounds. The synthesis of the samples with high compressive strength is an important result that highlights the diverse applications of these materials.

The results of flexural strength tests for Cu/Co-hybrid MOF/PVA fiber nanostructures are shown in Figure 9B. According to the data, Cu/Co-hybrid MOF/PVA fiber nanostructures have strength tests of about 16 N/mm^2. This amount is significant compared to previous polymers (Ngadiman et al., 2015; Su et al., 2022). The strengths of copper-containing MOF nanostructures I), cobalt-containing MOF nanostructures II), and Cu/Co-hybrid nanostructures III) were obtained as 5.6 N/mm^2, 1.9 N/mm^2, and 2.3 N/mm^2 respectively (**(n = 3) ± SD)**. The selection of optimal electrospinning conditions can affect the flexural strength tests of the final products. The different strengths of compounds I, II, and III can be related to the efficient effects of hybrid nanostructures on Cu/Co-hybrid nanostructures. The synthesis of compounds with high flexural strength tests can be used in different areas such as medicine, engineering, and tissue applications.

3.2 Catalyst activity of Cu/Co-hybrid MOF nanostructures

After identifying and confirming the structures of the Cu/Co-hybrid MOF nanostructures, they were used as a recoverable catalyst in the synthesis of pyrano[2,3-*c*]pyrazole derivatives (Scheme 1).

One of the important parameters in the synthesis and catalytic application of materials is their reusability. As mentioned in Section 2.5.2, after the synthesis of the derivatives, the nanoparticles were washed, dried, and used again in the synthesis of derivatives. The investigation into synthesis 5a showed that the catalyst could be recycled and reused five times without a noticeable decrease in efficiency (Figure 10).

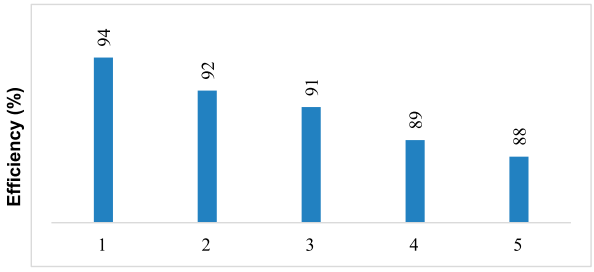

FIGURE 10
Recoverability of Cu/Co-hybrid MOF nanostructures as a catalyst in the synthesis of 4a.

The optimization of solvent, amount of catalyst, and temperature for the synthesis of pyrano[2,3-*c*]pyrazole derivatives were performed according to Table 2.

Optimum reaction conditions, including H_2O: EtOH (1:1) as the solvent, 3 mg Cu/Co-hybrid MOF, nanostructures as the catalyst, and a temperature of 40°C were obtained. Other pyrano[2,3-*c*] pyrazole derivatives under optimum conditions were synthesized according to Table 3.

For the synthesis of pyrano[2,3-*c*]pyrazole derivatives using Cu/Co-hybrid MOF nanostructures as a catalyst, the Scheme 2 mechanism can be proposed.

From the cyclization reaction of phenylhydrazine and ethyl acetoacetate, the pyrazole intermediate of I) is synthesized, which is in equilibrium with II). Intermediate III) is created from the condensation reaction of aldehyde derivatives and malononitrile. The Michael reaction of II) and III) leads to the creation of intermediate IV), which creates V) due to its intramolecular cyclization. Finally, with the tautomerization of V), the desired pyrano[2,3-*c*]pyrazole derivatives are synthesized.

The comparison of the synthesis of derivatives in different conditions (Table 4) shows that the nanocatalyst synthesized in this study has a higher ability than other reported methods, which can be attributed to the porosity and increased reactivity of nanoparticles.

10.3389/fmats.2023.1214426

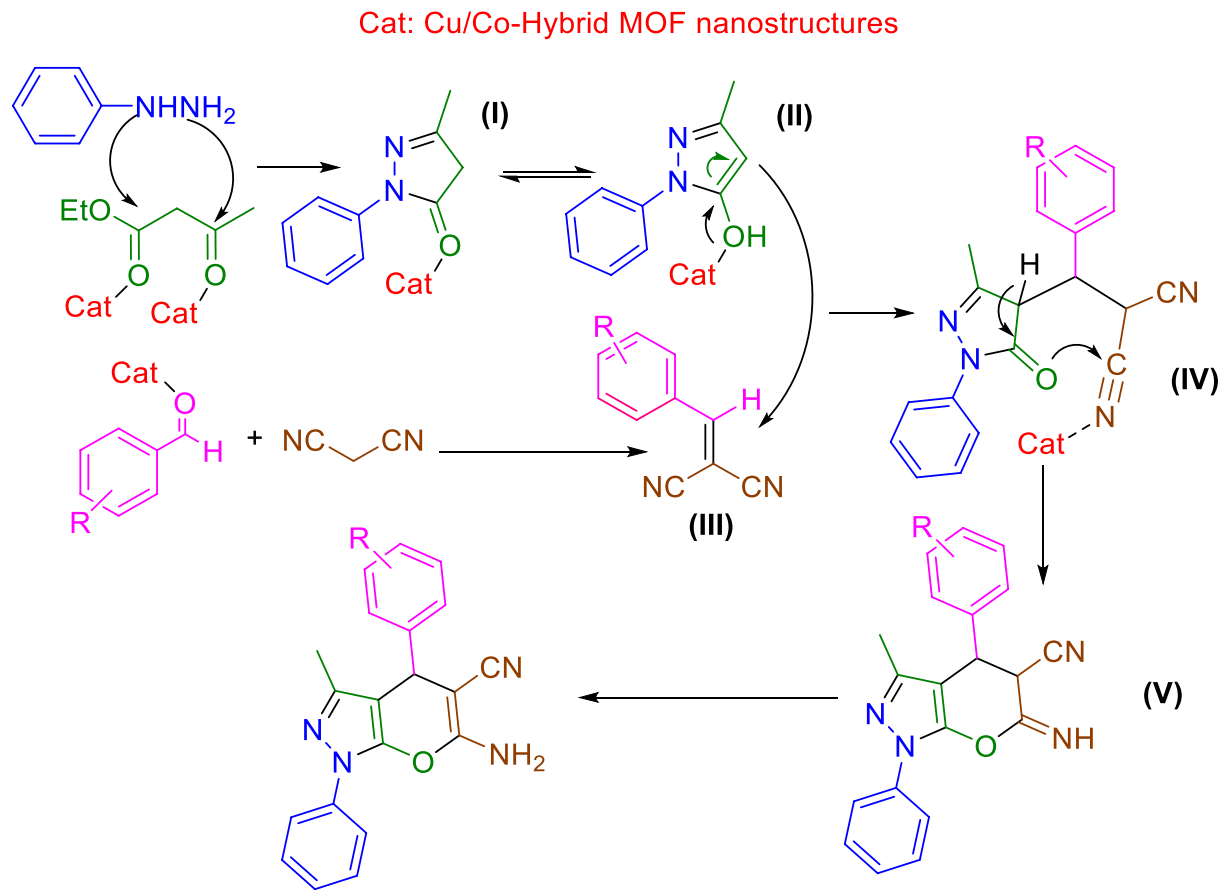

SCHEME 2
Proposed mechanisms for the synthesis of pyrano[2,3-c]pyrazole derivatives using Cu/Co-hybrid MOF nanostructures as a catalyst.

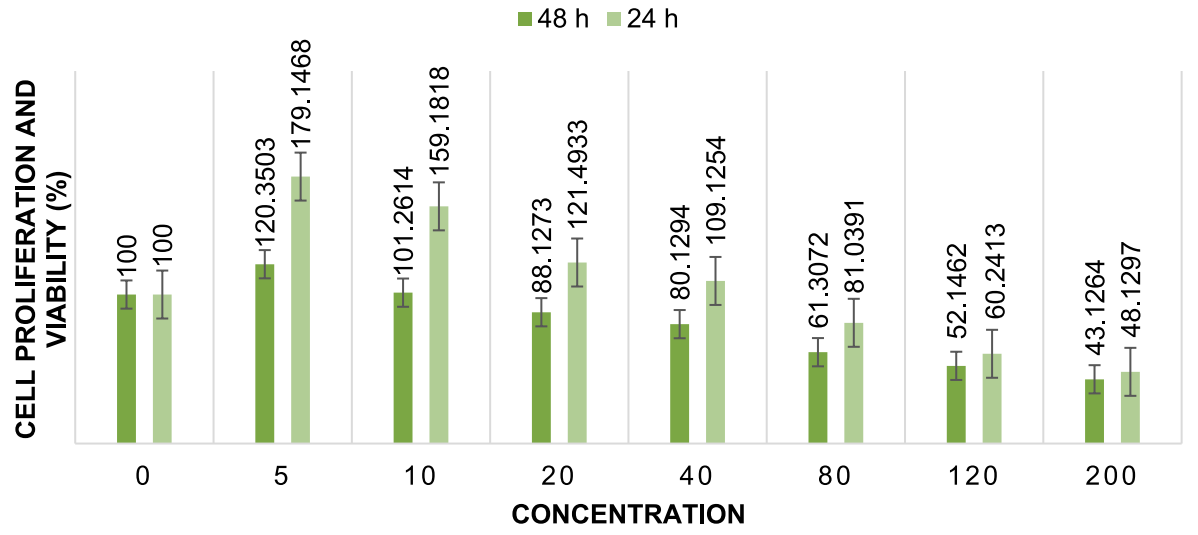

FIGURE 11
Cell proliferation and viability of Cu-MOF nanostructures at different concentrations after 24 h and 48 h (n = 3) ± SD.

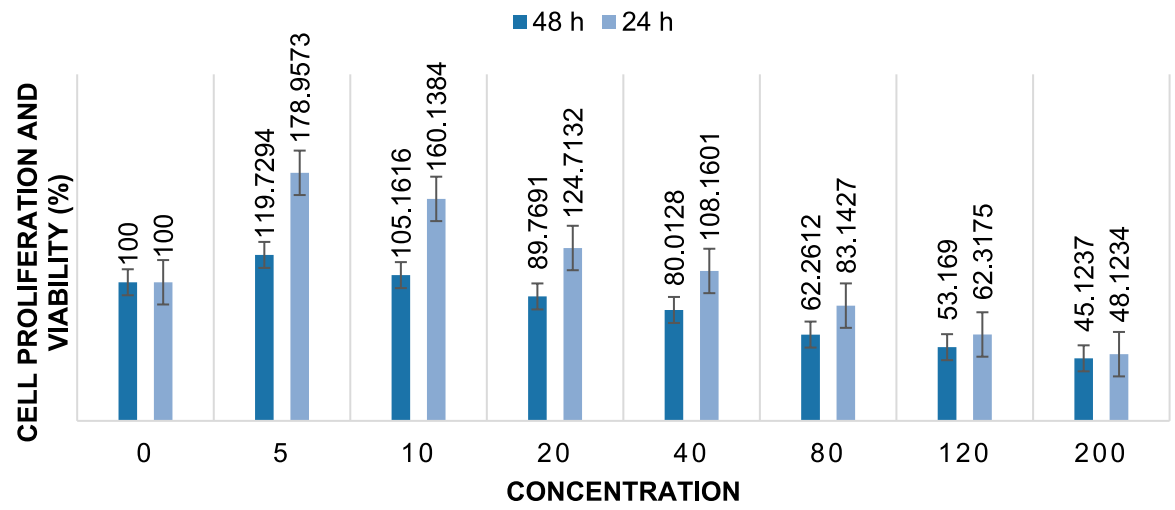

FIGURE 12
Cell proliferation and viability of Co-MOF nanostructures at different concentrations after 24 h and 48 h (n = 3) ± SD.

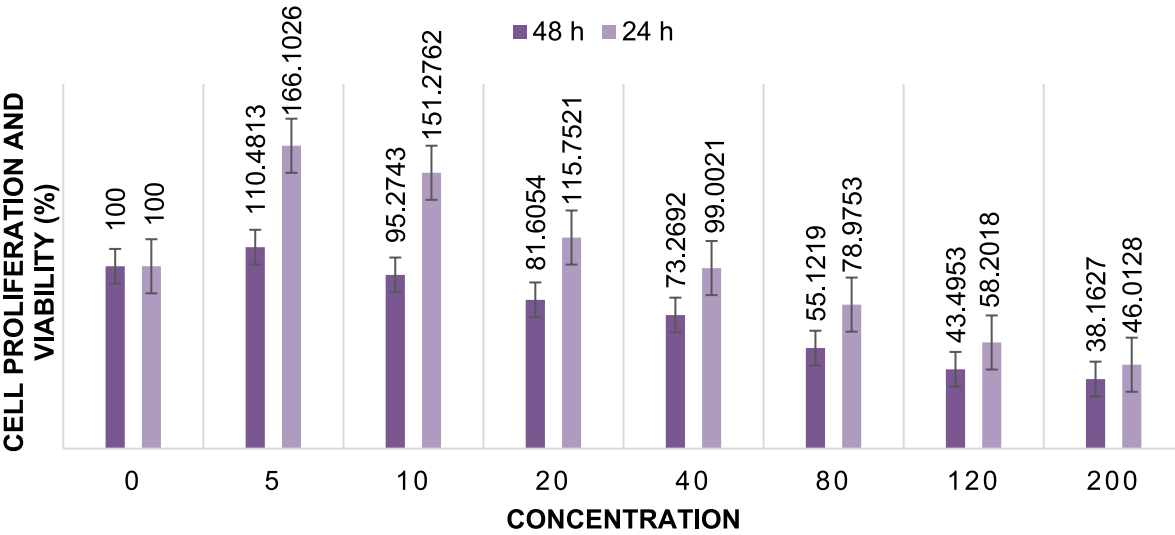

FIGURE 13
Cell proliferation and viability of Cu/Co-hybrid MOF nanostructures at different concentrations after 24 h and 48 h (n = 3) ± SD.

3.3 Cytotoxicity activity of Cu/Co-hybrid MOF nanostructures and Cu/Co-hybrid MOF/PVA fiber nanostructures

The cytotoxic activity of Cu/Co-hybrid MOF nanostructures and Cu/Co-hybrid MOF/PVA fiber nanostructures against MCF-7 breast cancer cells was evaluated. Investigations were carried out at 24 h and 48 h, in a concentration of 200 mg/mL; maximum cell proliferation and viability of 48%, 48%, 46%, and 41% compared to control were observed at 24 h for Cu-MOF nanostructures, Co-MOF nanostructures, Cu/Co-hybrid MOF nanostructures, and Cu/Co-hybrid MOF/PVA fiber nanostructures, respectively. At 48 h, cell proliferation and viability of 43%, 45%, 38%, and 30% compared to control were obtained for the Cu-MOF nanostructures, Co-MOF nanostructures, Cu/Co-hybrid MOF nanostructures, and Cu/Co-hybrid MOF/PVA fiber nanostructures, respectively (Figures 11–14). The tests were repeated three times, and the final result is the average of the results ((n = 3) ± SD).

Further, IC_{50} values were calculated at different times using the slope of the curve and the line equation for Cu/Co-hybrid MOF nanostructures and Cu/Co-hybrid MOF/PVA fiber nanostructures. The results showed that the IC_{50} for Cu-MOF nanostructures and Co-MOF nanostructures at 24 h and 48 h was 168 μg/mL, 169 μg/mL, and 148 μg/mL, 153 μg/mL, respectively. The IC_{50} for Cu/Co-hybrid MOF nanostructures at 24 h and 48 h was 163 μg/mL and 129 μg/mL, respectively. The IC_{50} for Cu/Co-hybrid MOF/PVA fiber nanostructures was 154 μg/mL and 115 μg/mL at 24 h and 48 h, respectively.

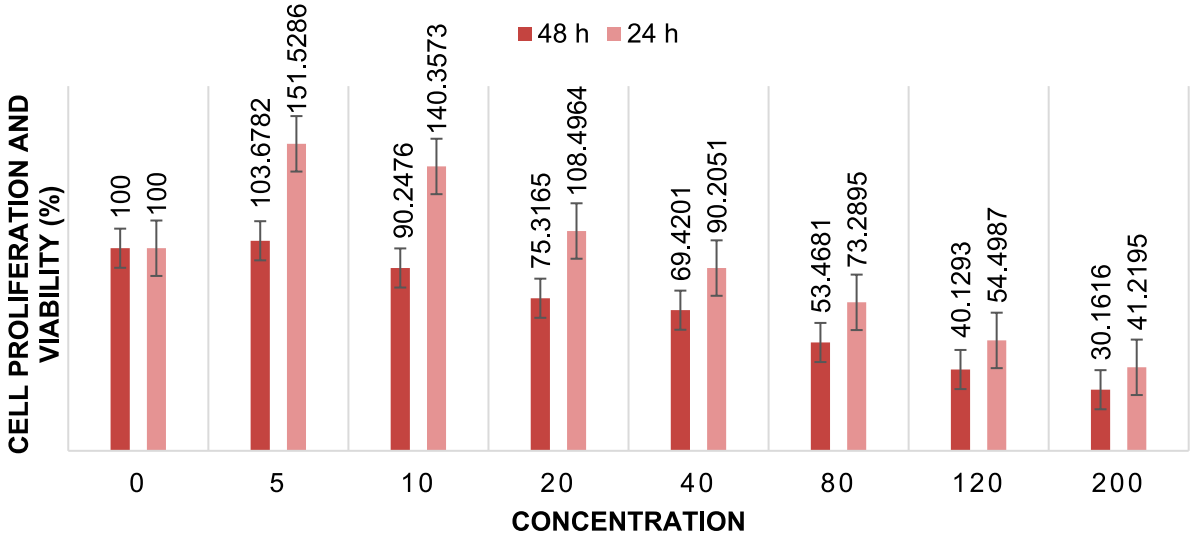

FIGURE 14
Cell proliferation and viability Cu/Co-hybrid MOF/PVA fiber nanostructures at different concentrations after 24 h and 48 h (n = 3) ± SD.

TABLE 5 Antibacterial and antifungal activities of copper-containing MOF nanostructures, cobalt-containing MOF nanostructures, Cu/Co-hybrid MOF nanostructures, and Cu/Co-hybrid MOF/PVA fiber nanostructures.

Product/drug	Gram-positive strain						Gram-negative strain						Fungal strain					
	A		B		C		D		E		F		G		H		I	
	I	II	I	II	I	II	I	II	I	II	I	II	I	III	I	III	I	III
Copper-containing MOFs	32	64	64	128	16	64	128	256	512	1024	-	-	16	64	256	512	32	64
Cobalt-containing MOFs	64	64	128	256	32	64	256	512	-	-	-	-	64	128	256	256	32	64
Cu/Co-hybrid MOFs	32	64	64	128	16	32	64	128	512	1024	-	-	64	64	128	256	32	32
Cu/Co-hybrid MOF/PVA	16	32	64	64	16	32	64	128	256	512	-	-	32	64	128	256	32	32
J	-	-	4	16	16	16	4	8	16	32	-	-	32	64	64	64	16	32
K	4	8	2	4	4	8	8	16	8	16	32	64	-	-	-	-	-	-

A: *Bacillus cereus*; B: *Staphylococcus aureus*; C: *Streptococcus pyogenes*; D: *Proteus mirabilis*; E: *Escherichia coli*; F: *Acinetobacter baumannii*; G: *Fusarium oxysporum*; H: *Candida albicans*; I: *Aspergillus fumigatus*. I: MIC (μg/mL); II: MBC (μg/mL); III: MFC (μg/mL). Drugs for bacteria: J: cefazolin, K: gentamicin; drug for fungi: J: terbinafine, K: tolnaftate. (n = 3) ± SD.

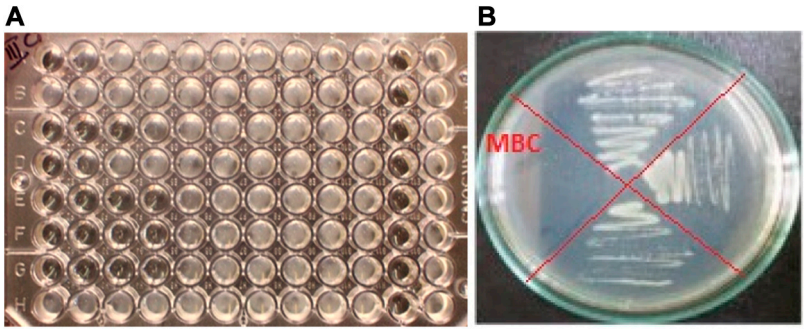

FIGURE 15
(A) MIC of Cu/Co-hybrid MOF/PVA on the studied strains, and **(B)** MBC of Cu/Co-hybrid MOF/PVA on *Escherichia coli*.

As evidenced by the results, the cytotoxicity activity of Cu/Co-hybrid MOF nanostructures and Cu/Co-hybrid MOF/PVA fiber nanostructures in 48 h is higher than it is at 24 h.

The results show that the cytotoxicity activity of Cu-MOF is very close to that of Co-MOF and slightly lower than that of the Cu/Co-hybrid MOF nanostructures. The increased activity of the Cu/Co-hybrid MOF nanostructures can be attributed to the formation of the hybrid of the Cu-MOF and Co-MOF nanostructures.

Comparing the cytotoxicity activity of Cu/Co-hybrid MOF nanostructures and Cu/Co-hybrid MOF/PVA fiber nanostructures shows that Cu/Co-hybrid MOF/PVA fiber nanostructures were more cytotoxically active. The greater effectiveness of Cu/Co-hybrid MOF/PVA fiber nanostructures can be attributed to BET, BJH pore volume, and mean pore diameter, as the results stated in Section 3.1. The cytotoxic activity of PVA fiber nanostructures was studied, and the results proved that the compound does not affect the studied cells.

From the results, it can be said that the cytotoxicity activity of Cu/Co-hybrid MOF nanostructures and Cu/Co-hybrid MOF/PVA fiber nanostructures depends on the duration of exposure and the porosity of the nanoparticles. The role of PVA fiber nanostructures is to increase porosity and, as a result, increase the effectiveness of the Cu/Co-hybrid MOF on the studied cells (Asgari et al., 2022; Sheta et al., 2022).

For Cu-MOF nanostructures, the *p*-value of IC_{50} at 24 h was 0.001 for concentrations. Thus, concentration is a critical parameter for this time. The *p*-value of IC_{50} at 48 h was 0.000 for concentrations. Thus, concentration is also a critical parameter for this time.

For Co-MOF nanostructures, the *p*-value of IC_{50} at 24 h was 0.002 for concentrations. Thus, concentration is a critical parameter for this time. The *p*-value of IC_{50} at 48 h was 0.001 for concentrations. Thus, concentration is a critical parameter for this time.

For Cu/Co-hybrid MOF nanostructures, the *p*-value of IC_{50} at 24 h is 0.000 for concentrations. Thus, concentration is a critical parameter for this time. The *p*-value of IC_{50} at 48 h was 0.004 for concentrations. Thus, concentration is a critical parameter for this time.

For Cu/Co-hybrid MOF/PVA fiber nanostructures, the *p*-value of IC_{50} at 24 h was 0.001 for concentrations. Thus, concentration is a critical parameter for this time. The *p*-value of IC_{50} at 48 h was 0.002 for concentrations. Thus, concentration is a critical parameter for this time.

As a final result, the IC_{50} depends on the concentration of compounds. Increasing the concentration increases the contact of molecules with the surface of the studied cells and increases the effectiveness.

3.4 Antimicrobial activity of Cu/Co-hybrid MOF nanostructures and Cu/Co-hybrid MOF/PVA fiber nanostructures

The antimicrobial activity (antibacterial and antifungal activities) of copper-containing MOF nanostructures, cobalt-containing MOF nanostructures, Cu/Co-hybrid MOF nanostructures, and Cu/Co-hybrid MOF/PVA fiber nanostructures was tested against *Bacillus cereus A)*, *Staphylococcus aureus B)*, and *Streptococcus pyogenes C)* as gram-positive species; *Proteus mirabilis D)*, *Escherichia coli E)*, and *Acinetobacter baumannii F)* as gram-negative species; and *Fusarium oxysporum G)*, *Candida albicans H)*, and *Aspergillus fumigatus I)* as fungal species. The results of the tests are given in Table 5 ((n = 3) ± SD).

In antibacterial and antifungal activities, minimum inhibitory concentration, minimum bactericidal concentration, and minimum fungicidal concentration were evaluated.

The porous structure of copper-containing MOF nanostructures, cobalt-containing MOF nanostructures, Cu/Co-hybrid MOF nanostructures, and Cu/Co-hybrid MOF/PVA fiber nanostructures had a strong effect on the studied species except for *E. coli* and *A. baumannii*. In some species, all three MOF compounds were more effective than commercial drugs (cefazolin for antibacterial activity and tolnaftate for antifungal activity).

As the laboratory observations in Table 2 show, Cu/Co-hybrid MOF nanostructures and Cu/Co-hybrid MOF/PVA fiber nanostructures have a better effect on the investigated bacterial and fungal species, which can be extended to the sum of the impacts of copper-containing MOF nanostructures and cobalt-containing MOFs.

The high antibacterial and antifungal activities of the synthesized Cu/Co-hybrid MOF nanostructures and Cu/Co-hybrid MOF/PVA fiber nanostructures can be attributed to the presence of nano-sized bioactive metals and their highly specific surface area (Asgari et al., 2022; Sheta et al., 2022).

The results of MIC of Cu/Co-hybrid MOF/PVA on the studied strains are shown as an example in Figure 15A, and in Figure 15B, the results of MBC of Cu/Co-hybrid MOF/PVA on *Escherichia coli* are given as an example.

4 Conclusion

In summary, copper-containing MOF nanostructures, cobalt-containing MOF nanostructures, and Cu/Co-hybrid MOF nanostructures were synthesized using the ultrasonic technique. By using Cu/Co-hybrid MOF nanostructures and PVA and electrospinning method, novel Cu/Co-hybrid MOF/PVA fiber nanostructures were synthesized. The structures of synthesized nanoparticles were identified and confirmed by BET, BJH, TGA, FTIR, SEM, and XRD. The catalytic properties of Cu/Co-hybrid MOF nanostructures in the synthesis of pyrano[2,3-*c*]pyrazole derivatives were investigated. The synthetic derivatives were synthesized with better efficiency and time. The cytotoxicity activity and antimicrobial (antibacterial and antifungal) effects of Cu/Co-hybrid MOF nanostructures and Cu/Co-hybrid MOF/PVA fiber nanostructures were investigated based on IC_{50} and cell proliferation and viability (for cytotoxicity evaluations), and MBC, MFC, and MIC (for antibacterial and antifungal evaluations). Antibacterial and antifungal effects were compared with the effects of known drugs. The result of the antibacterial and antifungal analyses showed that Cu/Co-hybrid MOF/PVA fiber nanostructures had better effects against some strains. The high antibacterial and antifungal activities of the synthesized nanostructures can be attributed to the presence of nano-sized bioactive metals and their high specific surface area.

In biological evaluations, the effectiveness of Cu/Co-hybrid MOF/PVA fiber nanostructures was higher than that of the Cu/Co-hybrid MOF nanostructures, which can be attributed to their BET and BJH volume pore and mean pore diameter.

Data availability statement

The original contributions presented in the study are included in the article/Supplementary material, further inquiries can be directed to the corresponding author.

Author contributions

Study conception and design, SH; data collection, MaA and YJ; analysis and interpretation of results, MoA and IM; draft manuscript preparation, ER, AA, and FA; editing, MS; visualization, SH and AA; project administration, MS. All authors contributed to the article and approved the submitted version.

Acknowledgments

The authors extend their appreciation to the Deanship of Scientific Research at King Khalid University for funding this work through the large research group program under grant number (R.G.P.02/148/43).

Conflict of interest

The authors declare that the research was conducted in the absence of any commercial or financial relationships that could be construed as a potential conflict of interest.

Publisher's note

All claims expressed in this article are solely those of the authors and do not necessarily represent those of their affiliated organizations, or those of the publisher, the editors, and the reviewers. Any product that may be evaluated in this article, or claim that may be made by its manufacturer, is not guaranteed or endorsed by the publisher.

References

Abdelmoaty, A. S., El-Beih, A. A., and Hanna, A. A. (2022). Synthesis, characterization and antimicrobial activity of copper-metal organic framework (Cu-MOF) and its modification by melamine. *J. Inorg. Organomet. Polym. Mater.* 32 (5), 1778–1785. doi:10.1007/s10904-021-02187-8

Adamu, B. F., Gao, J., Jhatial, A. K., and Kumelachew, D. M. (2021). A review of medicinal plant-based bioactive electrospun nano fibrous wound dressings. *Mater. Des.* 209, 109942. doi:10.1016/j.matdes.2021.109942

Ahmad, I., Jasim, S. A., Yasin, G., Al-Qargholi, B., and Hammid, A. T. (2022). Synthesis and characterization of new 1, 4-dihydropyran derivatives by novel Ta-MOF nanostructures as reusable nanocatalyst with antimicrobial activity. *Front. Chem.* 10, 967111. doi:10.3389/fchem.2022.967111

Akhavan-Sigari, R., Zeraati, M., Moghaddam-Manesh, M., Kazemzadeh, P., Hosseinzadegan, S., Chauhan, N. P. S., et al. (2022). Porous Cu-MOF nanostructures with anticancer properties prepared by a controllable ultrasound-assisted reverse micelle synthesis of Cu-MOF. *BMC Chem.* 16 (1), 10. doi:10.1186/s13065-022-00804-2

Alam, M. J., Alam, O., Alam, P., and Naim, M. J. (2015). A review on pyrazole chemical entity and biological activity. *Int. J. Pharm. Sci. Res.* 6, 1433–1442.

Almajhdi, F. N., Fouad, H., Khalil, K. A., Awad, H. M., Mohamed, S. H., Elsarnagawy, T., et al. (2014). *In-vitro* anticancer and antimicrobial activities of PLGA/silver nanofiber composites prepared by electrospinning. *J. Mater. Sci. Mater. Med.* 25, 1045–1053. doi:10.1007/s10856-013-5131-y

Amine Khodja, I., Fisli, A., Lebhour, O., Boulcina, R., Boumoud, B., and Debache, A. (2016). Four-component synthesis of pyrano [2, 3-c] pyrazoles catalyzed by triphenylphosphine in aqueous medium. *Lett. Org. Chem.* 13 (2), 1–91. doi:10.2174/1570178613666151207195411

Asgari, S., Ziarani, G. M., Badiei, A., Rostami, M., and Kiani, M. (2022). Reduced cytotoxicity and boosted antibacterial activity of a hydrophilic nano-architecture magnetic nitrogen-rich copper-based MOF. *Mater. Today Commun.* 33, 104393. doi:10.1016/j.mtcomm.2022.104393

Asiri, M., Abdulsalam, A. G., Kahtan, M., Alsaikhan, F., Farhan, I., Mutlak, D. A., et al. (2022). Synthesis of new zirconium magnetic nanocomposite as a bioactive agent and green catalyst in the four-component synthesis of a novel multi-ring compound containing pyrazole derivatives. *Nanomaterials* 12 (24), 4468. doi:10.3390/nano12244468

Azizabadi, O., Akbarzadeh, F., Danshina, S., Chauhan, N. P. S., and Sargazi, G. (2021a). An efficient ultrasonic assisted reverse micelle synthesis route for Fe3O4@ Cu-MOF/core-shell nanostructures and its antibacterial activities. *J. Solid State Chem.* 294, 121897. doi:10.1016/j.jssc.2020.121897

Azizabadi, O., Akbarzadeh, F., Sargazi, G., and Chauhan, N. P. S. (2021b). Preparation of a novel Ti-metal organic framework porous nanofiber polymer as an efficient dental nano-coating: physicochemical and mechanical properties. *Polymer-Plastics Technol. Mater.* 60 (7), 734–743. doi:10.1080/25740881.2020.1844231

Beter, M., Kara, H. K., Topal, A. E., Dana, A., Tekinay, A. B., and Guler, M. O. (2017). Multivalent presentation of cationic peptides on supramolecular nanofibers for antimicrobial activity. *Mol. Pharm.* 14 (11), 3660–3668. doi:10.1021/acs.molpharmaceut.7b00434

Bonan, R. F., Mota, M. F., da Costa Farias, R. M., da Silva, S. D., Bonan, P. R. F., Diesel, L., et al. (2019). *In vitro* antimicrobial and anticancer properties of TiO2 blow-spun nanofibers containing silver nanoparticles. *Mater. Sci. Eng. C* 104, 109876. doi:10.1016/j.msec.2019.109876

Chen, L., Zhang, X., Cheng, X., Xie, Z., Kuang, Q., and Zheng, L. (2020). The function of metal–organic frameworks in the application of MOF-based composites. *Nanoscale Adv.* 2 (7), 2628–2647. doi:10.1039/d0na00184h

Cui, W. G., Zhang, Q., Zhou, L., Wei, Z. C., Yu, L., Dai, J. J., et al. (2023). Hybrid MOF template-directed construction of hollow-structured In2O3@ ZrO2 heterostructure for enhancing hydrogenation of CO2 to methanol. *Small* 19 (1), 2204914. doi:10.1002/smll.202204914

Dam, B., Saha, M., and Pal, A. K. (2015). Magnetically recyclable nano-FDP: A novel, efficient nano-organocatalyst for the one-pot multi-component synthesis of pyran derivatives in water under ultrasound irradiation. *Catal. Lett.* 145 (9), 1808–1816. doi:10.1007/s10562-015-1586-4

Ding, M., Cai, X., and Jiang, H-L. (2019). Improving MOF stability: approaches and applications. *Chem. Sci.* 10 (44), 10209–10230. doi:10.1039/c9sc03916c

Dong, L-Z., Lu, Y-F., Wang, R., Zhou, J., Zhang, Y., Zhang, L., et al. (2022). Porous copper cluster-based MOF with strong cuprophilic interactions for highly selective electrocatalytic reduction of CO2 to CH4. *Nano Res.* 15 (12), 10185–10193. doi:10.1007/s12274-022-4681-z

Drelich, J. W., Boinovich, L., Chibowski, E., Della Volpe, C., Hołysz, L., Marmur, A., et al. (2019). Contact angles: history of over 200 years of open questions. *Surf. Innov.* 8 (1–2), 3–27. doi:10.1680/jsuin.19.00007

Dutta, B., Pal, K., Jana, K., Sinha, C., and Mir, M. H. (2019). Fabrication of a Zn (II)-Based 2D pillar bilayer metal-organic framework for antimicrobial activity. *ChemistrySelect* 4 (34), 9947–9951. doi:10.1002/slct.201901887

Eftekhari far, B., and Nasr-Esfahani, M. (2020). Synthesis, characterization and application of Fe3O4@ SiO2@ CPTMO@ DEA-SO3H nanoparticles supported on bentonite nanoclay as a magnetic catalyst for the synthesis of 1, 4-dihydropyrano [2, 3-c] pyrazoles. *Appl. Organomet. Chem.* 34 (3), e5406. doi:10.1002/aoc.5406

Elango, M., Deepa, M., Subramanian, R., and Mohamed Musthafa, A. (2018). Synthesis, characterization, and antibacterial activity of polyindole/Ag–Cuo nanocomposites by reflux condensation method. *Polymer-Plastics Technol. Eng.* 57 (14), 1440–1451. doi:10.1080/03602559.2017.1410832

Garazd, Y. L., and Garazd, M. (2016). Natural dibenzo [b, d] pyran-6-ones: structural diversity and biological activity. *Chem. Nat. Compd.* 52 (1), 1–18. doi:10.1007/s10600-016-1536-4

Ge, R., Ji, Y., Ding, Y., Huang, C., He, H., and Yu, D-G. (2023). Electrospun self-emulsifying core-shell nanofibers for effective delivery of paclitaxel. *Front. Bioeng. Biotechnol.* 11, 1112338. doi:10.3389/fbioe.2023.1112338

Gecgel, C., Gonca, S., Turabik, M., and Özdemir, S. (2022). An aluminum-based MOF and its amine form as novel biological active materials for antioxidant, DNA cleavage, antimicrobial, and biofilm inhibition activities. *Mater. Today Sustain.* 19, 100204. doi:10.1016/j.mtsust.2022.100204

Ghasemzadeh, M. A., Mirhosseini-Eshkevari, B., Tavakoli, M., and Zamani, F. (2020). Metal–organic frameworks: advanced tools for multicomponent reactions. *Green Chem.* 22 (21), 7265–7300. doi:10.1039/d0gc01767a

Gholami, A., Hashemi, S. A., Yousefi, K., Mousavi, S. M., Chiang, W-H., Ramakrishna, S., et al. (2020). 3D nanostructures for tissue engineering, cancer therapy, and gene delivery. *J. Nanomater.* 2020, 1–24. doi:10.1155/2020/1852946

Han, I., Choi, S. A., and Lee, D. N. (2022). Therapeutic application of metal–organic frameworks composed of copper, cobalt, and zinc: their anticancer activity and mechanism. *Pharmaceutics* 14 (2), 378. doi:10.3390/pharmaceutics14020378

Hassan, E. A., Yang, L., Elagib, T. H., Ge, D., Lv, X., Zhou, J., et al. (2019). Synergistic effect of hydrogen bonding and π-π stacking in interface of CF/PEEK composites. *Compos. Part B Eng.* 171, 70–77. doi:10.1016/j.compositesb.2019.04.015

Hatamie, S., Ahadian, M. M., Zomorod, M. S., Torabi, S., Babaie, A., Hosseinzadeh, S., et al. (2019). Antibacterial properties of nanoporous graphene oxide/cobalt metal organic framework. *Mater. Sci. Eng. C* 104, 109862. doi:10.1016/j.msec.2019.109862

Heidari Majd, M., Akbarzadeh, A., and Sargazi, A. (2017). Evaluation of host–guest system to enhance the tamoxifen efficiency. *Artif. cells, nanomedicine, Biotechnol.* 45 (3), 441–447. doi:10.3109/21691401.2016.1160916

Hosseinzadegan, S., Hazeri, N., Maghsoodlou, M. T., Moghaddam-Manesh, M., and Shirzaei, M. (2020). Synthesis and evaluation of biological activity of novel chromeno [4, 3-b] quinolin-6-one derivatives by SO 3 H-tryptamine supported on Fe 3 O 4@ SiO 2@ CPS as recyclable and bioactive magnetic nanocatalyst. *J. Iran. Chem. Soc.* 17 (12), 3271–3284. doi:10.1007/s13738-020-01990-3

Jasim, S. A., Hadi, J. M., Jalil, A. T., Opulencia, M. J. C., Hammid, A. T., Tohidimoghadam, M., et al. (2022). Electrospun Ta-MOF/PEBA nanohybrids and their CH4 adsorption application. *Front. Chem.* 10, 868794. doi:10.3389/fchem.2022.868794

Kalwar, K., and Shen, M. (2019). Electrospun cellulose acetate nanofibers and Au@AgNPs for antimicrobial activity-A mini review. *Nanotechnol. Rev.* 8 (1), 246–257. doi:10.1515/ntrev-2019-0023

Kang, S., Hou, S., Chen, X., Yu, D-G., Wang, L., Li, X., et al. (2020). Energy-saving electrospinning with a concentric teflon-core rod spinneret to create medicated nanofibers. *Polymers* 12 (10), 2421. doi:10.3390/polym12102421

Lismont, M., Dreesen, L., and Wuttke, S. (2017). Metal-organic framework nanoparticles in photodynamic therapy: current status and perspectives. *Adv. Funct. Mater.* 27 (14), 1606314. doi:10.1002/adfm.201606314

Liu, H., Bai, Y., Huang, C., Wang, Y., Ji, Y., Du, Y., et al. (2023). Recent progress of electrospun herbal medicine nanofibers. *Biomolecules* 13 (1), 184. doi:10.3390/biom13010184

Liu, N., Zhang, X., Guo, Q., Wu, T., and Wang, Y. (2022). 3D bioprinted scaffolds for tissue repair and regeneration. *Front. Mater.* 9, 925321. doi:10.3389/fmats.2022.925321

Luo, J., Ying, L-F., Zhang, F., Zhou, Z., and Zhang, Y-G. (2021). Cu (II)-containing metal–organic framework with 1D hexagonal channels for cyanosilylation reaction and anticancer activity on osteosarcoma cells. *ACS omega* 6 (8), 5856–5864. doi:10.1021/acsomega.0c06270

Maliszewska, I., and Czapka, T. (2022). Electrospun polymer nanofibers with antimicrobial activity. *Polymers* 14 (9), 1661. doi:10.3390/polym14091661

Moghaddam-manesh, M., Beyzaei, H., Heidari Majd, M., Hosseinzadegan, S., and Ghazvini, K. (2021). Investigation and comparison of biological effects of regioselectively synthesized thiazole derivatives. *J. Heterocycl. Chem.* 58, 1525–1530. doi:10.1002/jhet.4278

Moghaddam-Manesh, M., and Hosseinzadegan, S. (2021). Introducing new method for the synthesis of polycyclic compounds containing [1, 3] dithiine derivatives, with anticancer and antibacterial activities against common bacterial strains between aquatic and human. *J. Heterocycl. Chem.* 58 (11), 2174–2180. doi:10.1002/jhet.4345

Mu, C., and Wu, Q. (2017). Electrospun poly (ε-caprolactone) composite nanofibers with controlled release of cis-diamminediiodoplatinum for a higher anticancer activity. *Nanoscale Res. Lett.* 12, 318–8. doi:10.1186/s11671-017-2092-y

Ngadiman, N. H. A., Noordin, M., Idris, A., Shakir, A. S. A., and Kurniawan, D. (2015). Influence of polyvinyl alcohol molecular weight on the electrospun nanofiber mechanical properties. *Procedia Manuf.* 2, 568–572. doi:10.1016/j.promfg.2015.07.098

Nunes, P. S. G., Vidal, H. D. A., and Corrêa, A. G. (2020). Recent advances in catalytic enantioselective multicomponent reactions. *Org. Biomol. Chem.* 18 (39), 7751–7773. doi:10.1039/d0ob01631d

Patra, I., Ansari, M. J., Emad Izzat, S., Uktamov, K. F., Abid, M. K., Mahdi, A. B., et al. (2022). Synthesis of efficient Co-MOF as reusable nanocatalyst in the synthesis new 1, 4-dihydropyridine derivatives with antioxidant activity. *Front. Chem.* 943, 932902. doi:10.3389/fchem.2022.932902

Paul, S., Pradhan, K., Ghosh, S., De, S., and Das, A. R. (2014). Uncapped SnO2 quantum dot catalyzed cascade assembling of four components: A rapid and green approach to the pyrano [2, 3-c] pyrazole and spiro-2-oxindole derivatives. *Tetrahedron* 70 (36), 6088–6099. doi:10.1016/j.tet.2014.02.077

Sadasivan, S., Bellabarba, R. M., and Tooze, R. P. (2013). Size dependent reduction–oxidation–reduction behaviour of cobalt oxide nanocrystals. *Nanoscale* 5 (22), 11139–11146. doi:10.1039/c3nr02877a

Salavati-Niasari, M., Mir, N., and Davar, F. (2009). Synthesis and characterization of Co3O4 nanorods by thermal decomposition of cobalt oxalate. *J. Phys. Chem. Solids* 70 (5), 847–852. doi:10.1016/j.jpcs.2009.04.006

Sargazi, G., Ebrahimi, A. K., Afzali, D., Badoei-dalfard, A., Malekabadi, S., and Karami, Z. (2019). Fabrication of PVA/ZnO fibrous composite polymer as a novel sorbent for arsenic removal: design and a systematic study. *Polym. Bull.* 76 (11), 5661–5682. doi:10.1007/s00289-019-02677-3

Sedighinia, E., Badri, R., and Kiasat, A. (2019). Application of yttrium iron garnet as a powerful and recyclable nanocatalyst for one-pot synthesis of pyrano [2, 3-c] pyrazole derivatives under solvent-free conditions. *Russ. J. Org. Chem.* 55 (11), 1755–1763. doi:10.1134/s1070428019110186

Shahryari, T., Alizadeh, V., Kazemzadeh, P., Jadoun, S., Chauhan, N. P. S., and Sargazi, G. (2022). A controllable procedure for removing Navicula algae from drinking water using an ultrasonic-assisted electrospun method for highly efficient synthesis of Co-MOF/PVA polymeric network. *Appl. Phys. A* 128 (5), 396. doi:10.1007/s00339-022-05524-x

Shahryari, T., Vahidipour, F., Chauhan, N. P. S., and Sargazi, G. (2020). Synthesis of a novel Zn-MOF/PVA nanofibrous composite as bioorganic material: design, systematic study and an efficient arsenic removal. *Polym. Eng. Sci.* 60 (11), 2793–2803. doi:10.1002/pen.25510

Sheta, S. M., Salem, S. R., and El-Sheikh, S. M. (2022). A novel iron (III)-based MOF: synthesis, characterization, biological, and antimicrobial activity study. *J. Mater. Res.* 37 (14), 2356–2367. doi:10.1557/s43578-022-00644-9

Sikandar, S., and Zahoor, A. F. (2021). Synthesis of pyrano [2, 3-c] pyrazoles: A review. *J. Heterocycl. Chem.* 58 (3), 685–705. doi:10.1002/jhet.4191

Sridhar, R., Venugopal, J., Sundarrajan, S., Ravichandran, R., Ramalingam, B., and Ramakrishna, S. (2011). Electrospun nanofibers for pharmaceutical and medical applications. *J. drug Deliv. Sci. Technol.* 21 (6), 451–468. doi:10.1016/s1773-2247(11)50075-9

Su, S., Hu, S., and Liu, Q. (2022). Application of polypyrrole cellulose nanocrystalline composite conductive material in garment design. *Adv. Mater. Sci. Eng.* 2022, 1–11. doi:10.1155/2022/4187826

Teixeira, A. P. C., Purceno, A. D., Barros, A. S., Lemos, B. R., Ardisson, J. D., Macedo, W. A., et al. (2012). Amphiphilic magnetic composites based on layered vermiculite and fibrous chrysotile with carbon nanostructures: application in catalysis. *Catal. today* 190 (1), 133–143. doi:10.1016/j.cattod.2012.01.042

Tipale, M. R., Khillare, L. D., Deshmukh, A. R., and Bhosle, M. R. (2018). An efficient four component domino synthesis of pyrazolopyranopyrimidines using recyclable choline chloride: urea deep eutectic solvent. *J. Heterocycl. Chem.* 55 (3), 716–728. doi:10.1002/jhet.3095

Uddin, M. K., and Baig, U. (2019). Synthesis of Co3O4 nanoparticles and their performance towards methyl orange dye removal: characterisation, adsorption and response surface methodology. *J. Clean. Prod.* 211, 1141–1153. doi:10.1016/j.jclepro.2018.11.232

Wang, M., Ge, R., Zhao, P., Williams, G. R., Yu, D-G., and Bligh, S. A. (2023). Exploring wettability difference-driven wetting by utilizing electrospun chimeric Janus microfiber comprising cellulose acetate and polyvinylpyrrolidone. *Mater. Des.* 226, 111652. doi:10.1016/j.matdes.2023.111652

Wang, M., Hou, J., Yu, D-G., Li, S., Zhu, J., and Chen, Z. (2020). Electrospun tri-layer nanodepots for sustained release of acyclovir. *J. Alloys Compd.* 846, 156471. doi:10.1016/j.jallcom.2020.156471

Wu, M., Feng, Q., Wan, D., and Ma, J. (2013). CTACl as catalyst for four-component, one-pot synthesis of pyranopyrazole derivatives in aqueous medium. *Synth. Commun.* 43 (12), 1721–1726. doi:10.1080/00397911.2012.666315

Wu, T., Liu, X., Liu, Y., Cheng, M., Liu, Z., Zeng, G., et al. (2020). Application of QD-MOF composites for photocatalysis: energy production and environmental remediation. *Coord. Chem. Rev.* 403, 213097. doi:10.1016/j.ccr.2019.213097

Yang, R-G., Fu, Y-M., Meng, X., Xue, L., Zhou, Z., He, Y-O., et al. (2023). Novel COF@ Ti–MOF hybrid photocatalysts enabling enhanced photocatalytic CO 2 reduction in a gas–solid system without additives. *Inorg. Chem. Front.* 10 (12), 3699–3705. doi:10.1039/d3qi00217a

Yoon, J. W., Seo, Y. K., Hwang, Y. K., Chang, J. S., Leclerc, H., Wuttke, S., et al. (2010). Controlled reducibility of a metal–organic framework with coordinatively unsaturated sites for preferential gas sorption. *Angew. Chem. Int. Ed.* 49 (34), 5949–5952. doi:10.1002/anie.201001230

Yu, D-G., Li, Q., Song, W., Xu, L., Zhang, K., and Zhou, T. (2023). Advanced technique-based combination of innovation education and safety education in higher education. *J. Chem. Educ.* 100, 507–516. doi:10.1021/acs.jchemed.2c00568

Zeraati, M., Moghaddam-Manesh, M., Khodamoradi, S., Hosseinzadegan, S., Golpayegani, A., Chauhan, N. P. S., et al. (2022). Ultrasonic assisted reverse micelle synthesis of a novel Zn-metal organic framework as an efficient candidate for antimicrobial activities. *J. Mol. Struct.* 1247, 131315. doi:10.1016/j.molstruc.2021.131315

Zha, Q., Yuan, F., Qin, G., and Ni, Y. (2020). Cobalt-based MOF-on-MOF two-dimensional heterojunction nanostructures for enhanced oxygen evolution reaction electrocatalytic activity. *Inorg. Chem.* 59 (2), 1295–1305. doi:10.1021/acs.inorgchem.9b03011

Zhang, M., Wang, G., Zhang, X., Zheng, Y., Lee, S., Wang, D., et al. (2021). Polyvinyl alcohol/chitosan and polyvinyl alcohol/Ag@ MOF bilayer hydrogel for tissue engineering applications. *Polymers* 13 (18), 3151. doi:10.3390/polym13183151

Zhang, M., Zhao, X., Zhang, G., Wei, G., and Su, Z. (2017). Electrospinning design of functional nanostructures for biosensor applications. *J. Mater. Chem. B* 5 (9), 1699–1711. doi:10.1039/c6tb03121h

Zhao, P., Chen, W., Feng, Z., Liu, Y., Liu, P., Xie, Y., et al. (2022). Electrospun nanofibers for periodontal treatment: A recent progress. *Int. J. Nanomedicine* 17, 4137–4162. doi:10.2147/ijn.s370340

Zhou, Y., Wang, M., Yan, C., Liu, H., and Yu, D-G. (2022). Advances in the application of electrospun drug-loaded nanofibers in the treatment of oral ulcers. *Biomolecules* 12 (9), 1254. doi:10.3390/biom12091254